Supporting Information

Coupling Porous Ni Doped $LaFeO_3$ nanoparticle with Amorphous FeOOH Nanosheet Yields Interfacial Electrocatalyst for Electrocatalytic Oxygen Evolution

Yanxin Li,[a] Xiaoyan Zhang,[a] Zhijing Wu,[a] Hongbin Sheng,[a] Can Li,*[b] Haiyan Li,[a] Lixin Cao,*[a] Bohua Dong*[a]

[a] School of Materials Science and Engineering, Ocean University of China, 238 Songling Road, Qingdao, 266100 P. R. China. E-mail: dongbohua@ouc.edu.cn ; caolixin@ouc.edu.cn

[b] Institute of Optoelectronic Materials and Devices, College of Optical and electronic Technology, China Jiliang Unicersity, 256 Xueyuan Street, Hangzhou, Zhejiang 310000, P.R. China. E-mail: canli1983@gmail.com

EXPERIMENTAL SECTION

Synthesis of Porous LFO.

All the chemicals used in the experiments were analytical grade (AR) without purification. Porous LFO powder was synthesized using a combined ethylenediaminetetraacetic acid (EDTA)-citrate complexing hydrothermal process. Briefly, 1.732g $La(NO_3)_3 \cdot 6H_2O$ and 1.616g $Fe(NO_3)_3 \cdot 9H_2O$ (Sinopharm Chemical Reagent Co., Ltd.) were dissolved in 40 mL ethylene glycol (Sinopharm Chemical Reagent Co., Ltd.). Then, 1.69 g EDTA ($C10H16N_2O_8$, Sinopharm Chemical Reagent Co., Ltd.) was added into the mixed solution, then an aqueous ammonium hydroxide solution ($NH_3 \cdot H_2O$, 28%, Sinopharm Chemical Reagent Co., Ltd.) was added to adjust the solution pH value to approximately 6. The resulting solution was stirred for 40 minutes continuously at room tempreture. Further, the mixed solution was transferred to a 100 mL Teflon-lined stainless steel autoclave a piece of Ni foam was placed vertically in the autoclave and heated at 180 ℃ for 24 hours, then

naturally cooled to room temperature. Then, the product Ni foam was washed with deionized water and dried at 60 ℃ for 6 h. Finally, the Ni foam was calcinated in air at 500 ℃ for 4 h to obtain the porous LFO. LNO was prepared via the same progress except that $Fe(NO_3)_2 \cdot 9H_2O$ was replaced by $Ni(NO_3)_2 \cdot 9H_2O$.

Synthesis of LFO Nps.

LFO Nps was synthesized by a traditional sol-gel route. Briefly, 1.732g $La(NO_3)_3 \cdot 6H_2O$ and 1.616g $Fe(NO_3)_2 \cdot 6H_2O$ were dissolved in 50 mL deionized (DI) water. followed by the addition of citric acid ($C_6H_8O_7$, Sinopharm Chemical Reagent Co., Ltd.) at a molar ratio of 1:2 for the total metal ion/ citric acid. Then, $NH_3 \cdot H_2O$ was added to adjust the solution pH value to approximately 6. The solution was continuously stirred and evaporated at 80 ℃ to yield a gel in brick red. Further, the gel was heated in the oven at 120 ℃ for 6 h to obtain the solid precursor. Finally, the solid precursor was calcinated in air at 600 ℃ for 4 h to obtain the LFO Nps powder.

Synthesis of NiFe-LFO.

First, the Ni foam with porous LFO was immersed in the mixed solution containing 30 mM $FeCl_3 \cdot 9H_2O$, $NiCl_2 \cdot 6H_2O$ and 45 mM urea (Sinopharm Chemical Reagent Co., Ltd.) with different $[Ni^{2+}]/[Fe^{3+}]$ ratios for 45 min at 100 ℃. Then, the coated Ni foam was rinsed with DI water and air-dried.

Synthesis of Ni-LFO.

The Ni-LFO was synthesized by hydrothermal process. Briefly, the Ni foam with porous LFO was immersed in the mixed solution containing $NiCl_2 \cdot 6H_2O$ and 45 mM urea for 45 min at 100 ℃. Then, the coated Ni foam was rinsed with DI water and air-dried.

Synthesis of LNO-FeOOH.

The LNO-FeOOH was synthesized through the following process, Briefly, 1.732g $La(NO_3)_3 \cdot 6H_2O$, 1.616g $Ni(NO_3)_3 \cdot 9H_2O$ and 1.69 g EDTA were dissolved in 40 mL ethylene

glycol, then an aqueous ammonium hydroxide solution was added to adjust the solution pH value to approximately 6. The resulting solution was stirred for 40 minutes continuously at room tempreture. Further, the mixed solution was transferred to a 100 mL Teflon-lined stainless steel autoclave a piece of Ni foam was placed vertically in the autoclave and heated at 180 ℃ for 24 hours, then naturally cooled to room temperature. Then, the product Ni foam was washed with deionized water and dried at 60 ℃ for 6 h. Finally, the Ni foam was calcinated in air at 500 ℃ for 4 h to obtain the LNO. Then, the Ni foam with porous NFO was immersed in solution containing 30 mM $FeCl_3 \cdot 9H_2O$ and 45 mM urea for 45 min at 100 ℃. Then, the coated Ni foam was rinsed with DI water and air-dried.

Physicochemical Characterization.

Transmission electron microscopy (TEM) images, high resolution TEM images and electron diffraction patterns were measured with a JEOL JEM-3200FS. The samples were prepared by sonication the catalysts off from the Ni foam, then the suspensions with catalyst were dropped onto the copper grid for TEM, SAED pattern and HRTEM characterization. X-ray diffraction data was collected on a diffractometer (D8 Advance, Bruker) with Cu Kα radiation (2θ ranging from 20° to 80°, λ = 1.541 Å, step size = 0.02°). X-ray photoelectron spectroscopy (XPS) studies were carried out on ESCALAB 250Xi (Thermo Fisher). Spectra were analyzed using XPS PEAK software, and the C1s peak for adventitious hydrocarbons at 284.8 eV was used for binding energy calibration. Elemental contents of the samples were measured by inductively coupled plasmaatomic emission spectrometer (ICP-AES, Arcos II MV). The specific surface areas and the corresponding pore size distribution of the samples were measured on a Quadrasorb SI-MP system at 77 K.

Electrochemical Measurements.

Electrochemical measurements were conducted with a standard three-electrode configuration by the CHI760E electrochemistry workstation. A Hg/HgO electrode was used as the reference electrode, and a Pt wire was used as the counter electrode. The working electrodes were LFO, Ni-LFO, NiLFO-FeOOH, LNOand NiFe-LFO catalysts. The potentials were calibrated against the RHE according to the following equation: (E_{RHE} = *0.098 V+0.059pH, 25 ℃*), pH is the pH of the electrolyte solution, and E_{RHE} is the calibrated potential. The polarization curves were obtained using linear sweep voltammetry (LSV) with a scan rate of 5 mV/s, and were corrected with iR (90%, Ru ca. 2 Ω) correction. Electrochemical impedance spectroscopy (EIS) analysis were conducted at 0.6 V vs Hg/HgO at overpotential of 220 mV at DC potential of 5 mV with the frequency ranging from 100 kHz to 0.1 Hz. Tafel plots were collected from the steady-state LSV measurements at a scan rate of 5 mV s-1. All experiments were performed at room temperature.

Calculation of active sites:

CV measurements were measured at 50 mV s^{-1} in 1 M solution PBS (pH = 7.0). Later, the absolute components of the voltammetric charges (cathodic and anodic) reported during one single blank measurement were added. Assuming a one electron redox process, this absolute charge was divided by two. The value was then divided by the Faraday constant to get the number of active sites (N) of catalysts.

$$N = \frac{Q}{2F} = \frac{\int IV/\nu}{2F}$$

Q: the CV charge capacity obtained by integrating the CV curves.

F: Faraday constant (96485 C/mol).

I: current density (A)

V: voltage (V vs RHE)

ν: scan rate (V s^{-1})

TOF calculation:

$$TOF = \frac{1}{FN} * \frac{1}{4}$$

I: Current (A) during the LSV measurement in 1.0 M KOH.

F: Faraday constant (96485 C/mol).

N: Number of active sites (mol).

The factor 1/4 arrives by taking into account that four electrons are required to form one oxygen molecule.

DFT calculations

The surfaces of $LaFeO_3$(111), FeOOH (110)+$LaFeO_3$(111) and FeOOH (110)+$LaNiFeO_3$(111) were been built, where the vacuum space along the z direction is set to be 20 Å, which is enough to avoid interaction between the two neighboring images. Then the OH, O and OOH groups have been adsorbed on the surface. The bottom three atomic layers were fixed, the top three atomic layers were relaxed adequately for all systems. The first principles calculations in the framework of density functional theory were carried out based on the Cambridge Sequential Total Energy Package known as CASTEP.[1] The exchange–correlation functional under the generalized gradient approximation (GGA) [2] with norm-conserving pseudopotentials and Perdew–Burke–Ernzerhof functional was adopted to describe the electron–electron interaction.[3] An energy cutoff of 750 eV was used and a k-point sampling set of 5 x 5 x 1 were tested to be converged. A force tolerance of 0.01 eV $Å^{-1}$, energy tolerance of $5.0x10^{-7}$eV per atom and maximum displacement of $5.0x10^{-4}$ Å were considered.

1. M. D. Segall, P. J. D. L. M. J. Probert, C. J. Pickard, P. J. Hasnip, S. J. Clark and M. C. Payne, *J. Phys.: Condens. Matter*, 2002, 14, 2717.

2. J. P. Perdew, K. Burke and M. Ernzerhof, *Phys. Rev. Lett.*, 1996,77, 3865.

3. D. R. Hamann, M. Schl¨ uter and C. Chiang, *Phys. Rev. Lett*., 1979,43, 1494.

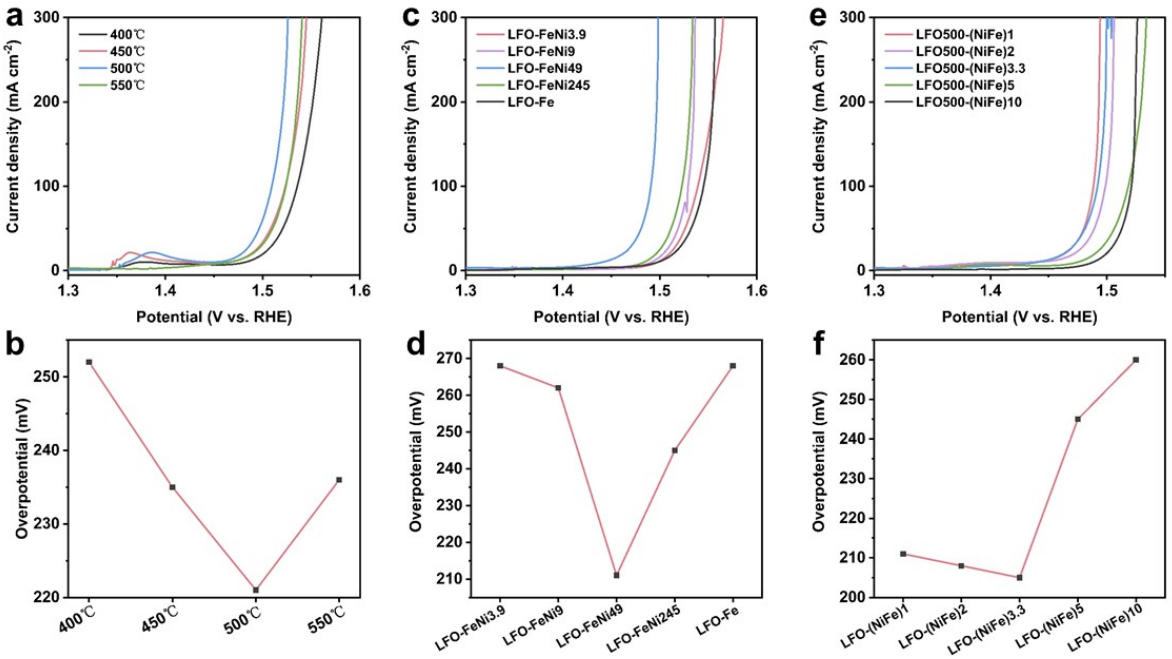

Figure S1. Optimization of experimental conditions: a, b) calcination temperature; c,d)

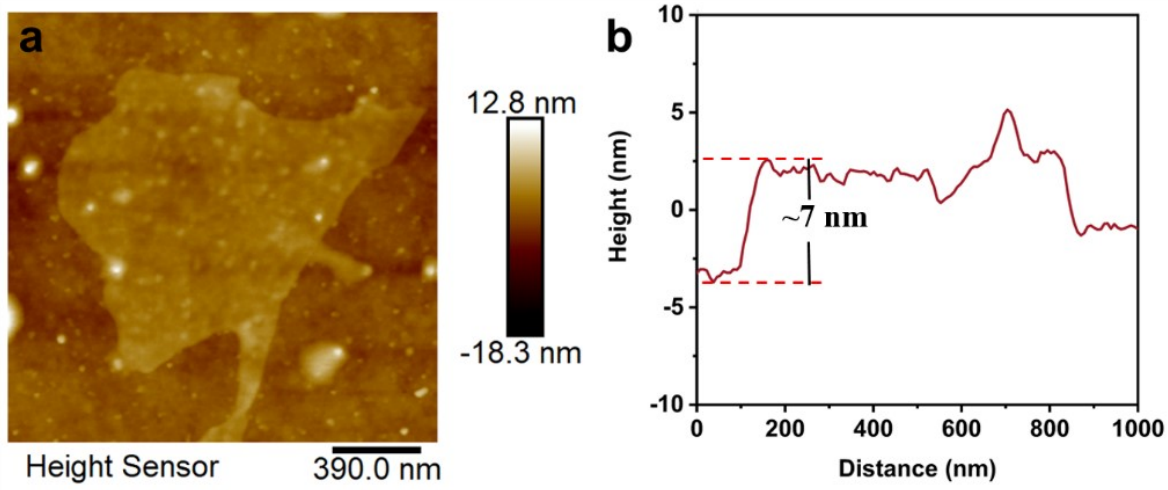

Figure S2. a) AFM pattern of the FeOOH ultrathin nanosheets. b) The thickness of FeOOH ultrathin nanosheets.

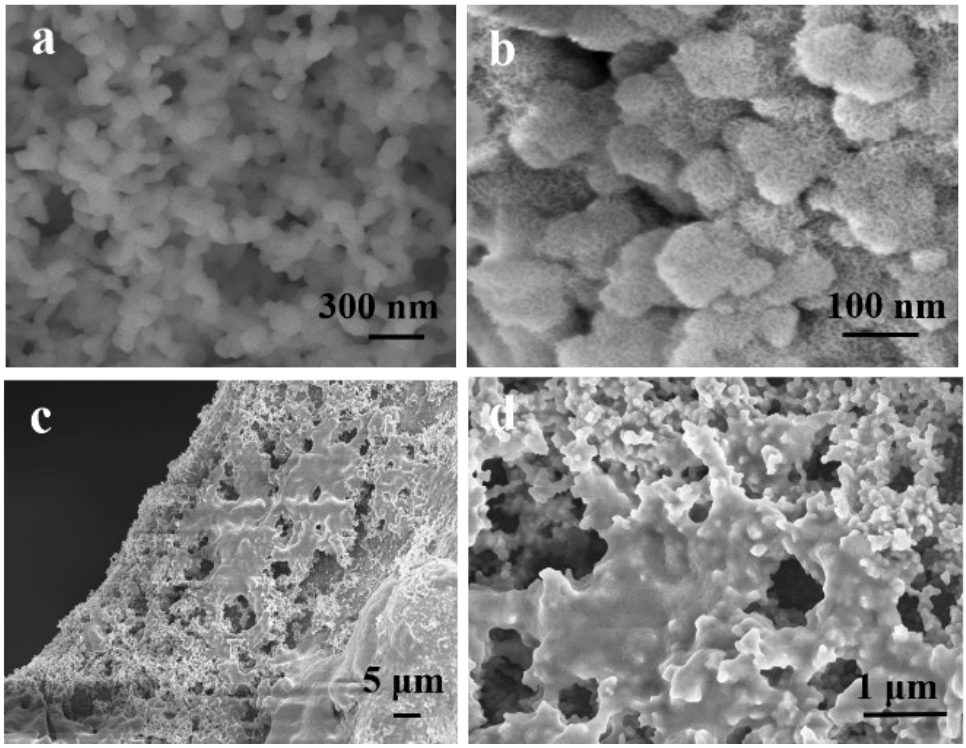

Figure S3. SEM images of a, b) pure LFO; c, d) NiFe-LFO.

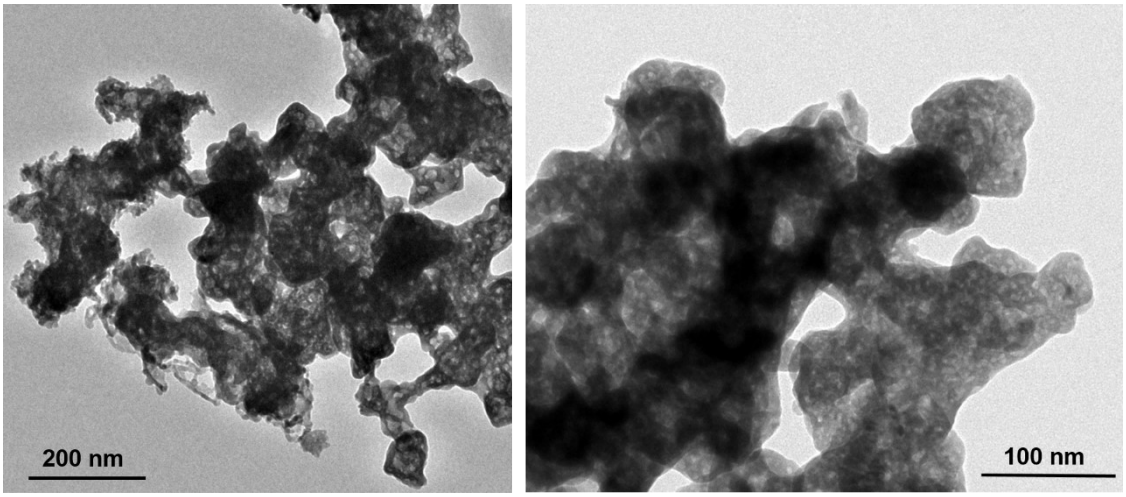

Figure S4. TEM images of Ni-doped LFO.

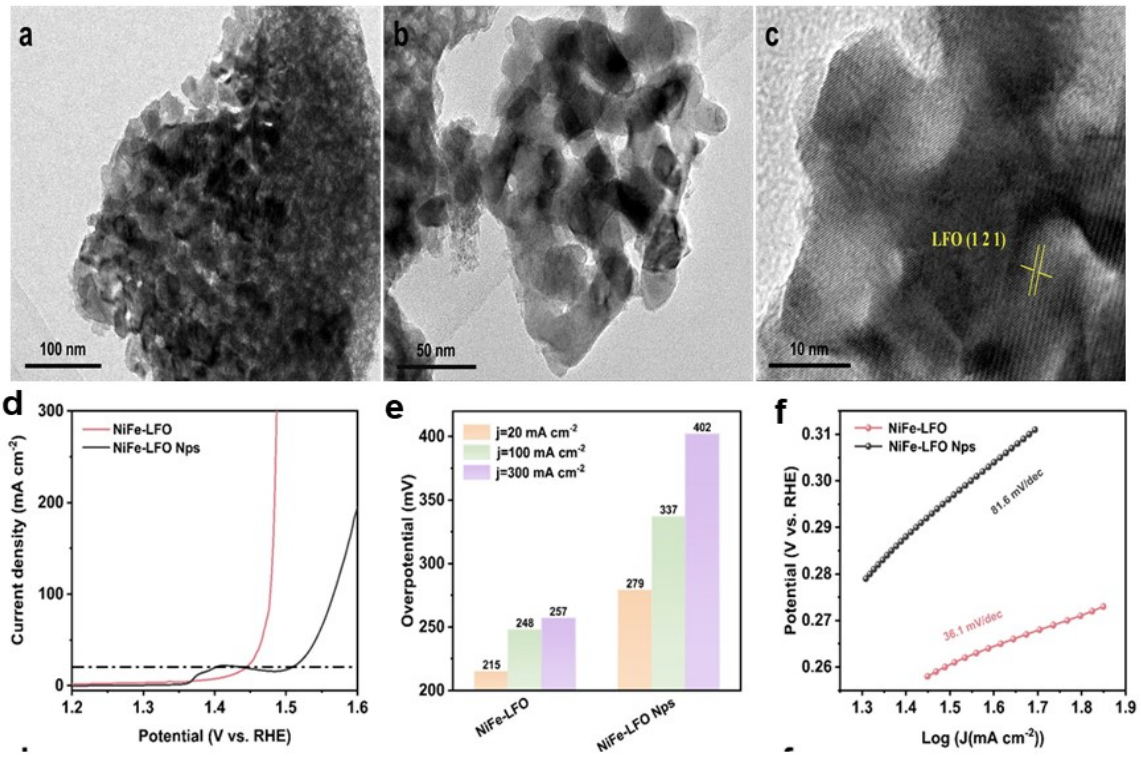

Figure S5. a, b, c) TEM images of pure LFO Nps and NiFe-LFO Nps; d) LSV curves, e) overpotentials at 10, 100 and 300 mA cm^{-2}, f) Tafel slopes of NiFe-LFO and NiFe-LFO Nps.

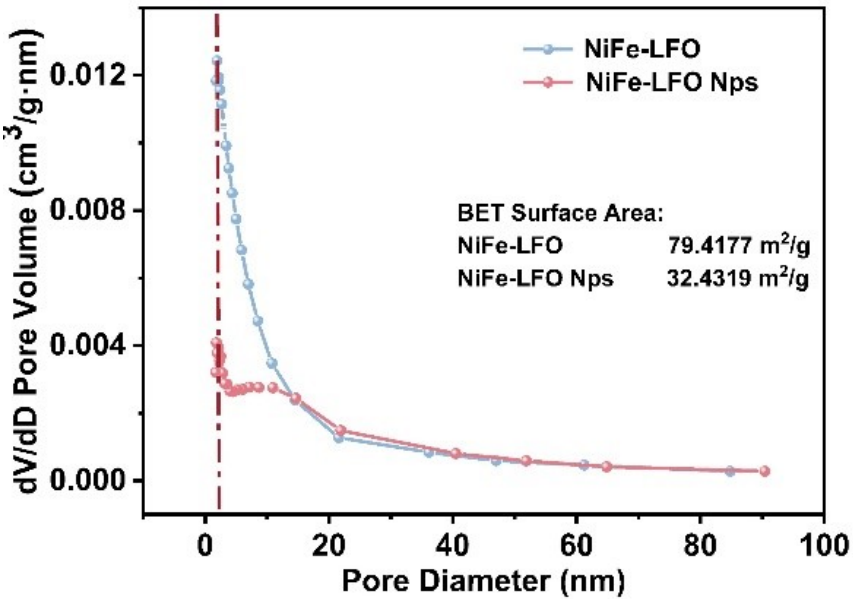

Figure S6. pore sizes, specific surface area of NiFe-LFO and NiFe-LFO Nps.

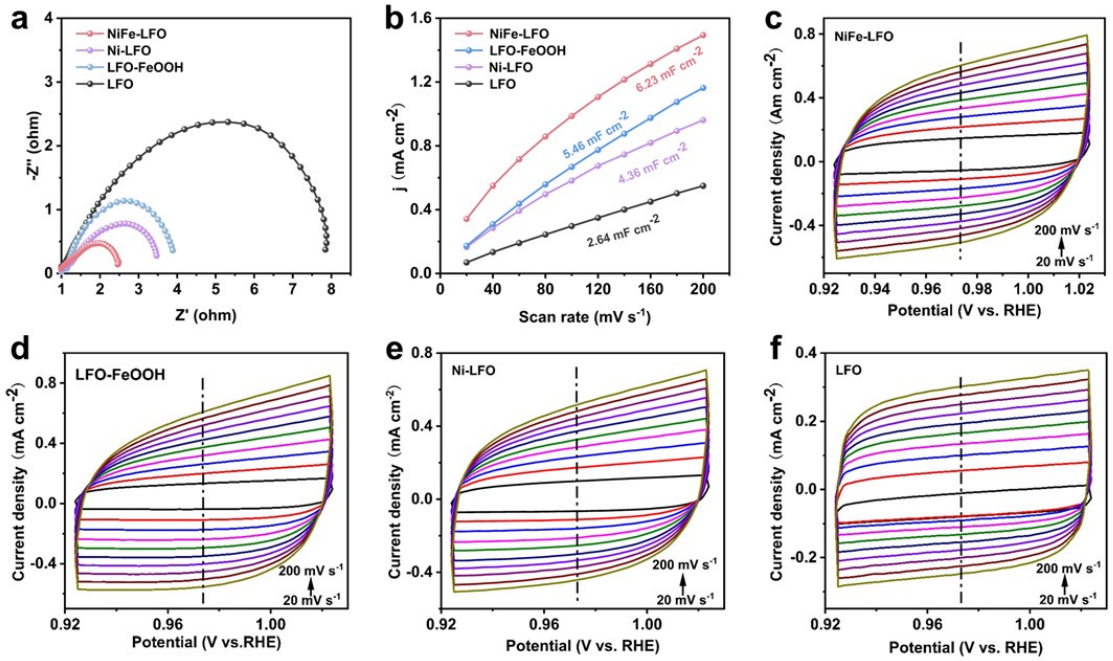

Figure S7. a) EIS Plots; b, c, d, e, f) Cdl of pure LFO, LFO-FeOOH, Ni-LFO and NiFe-LFO.

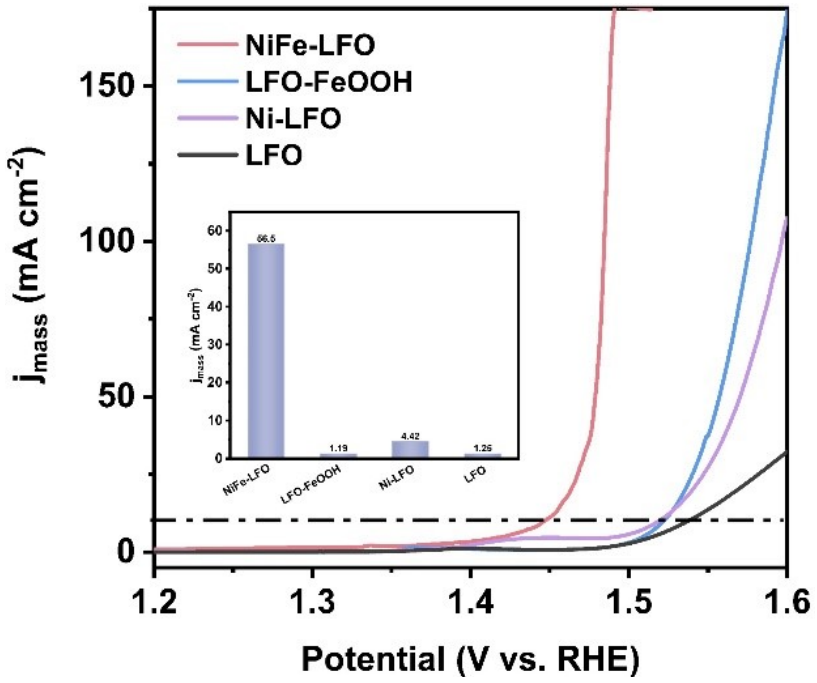

Figure S8. mass activity of LFO, Ni-LFO, LFO-FeOOH and NiFe-LFO.

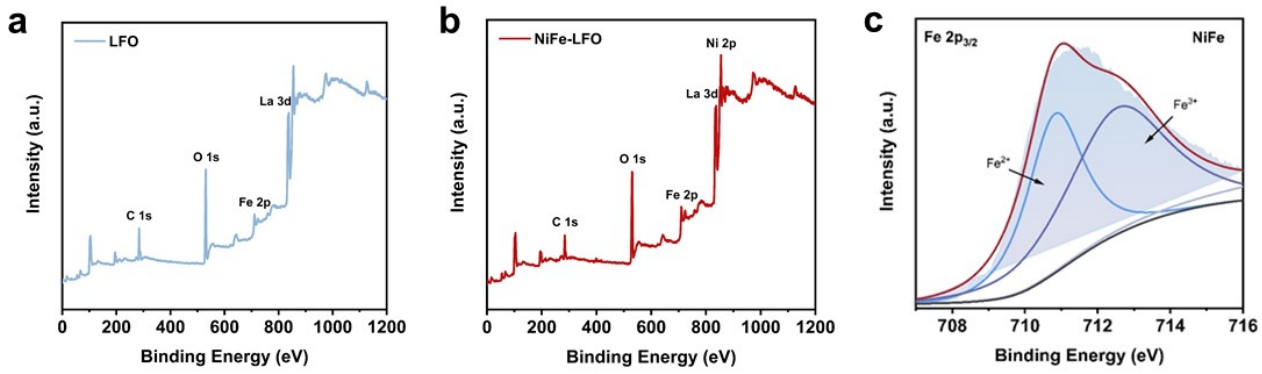

Figure S9. a, b) XPS survey of LFO and Ni- LFO; c) Fe $2p_{3/2}$ of NiFe.

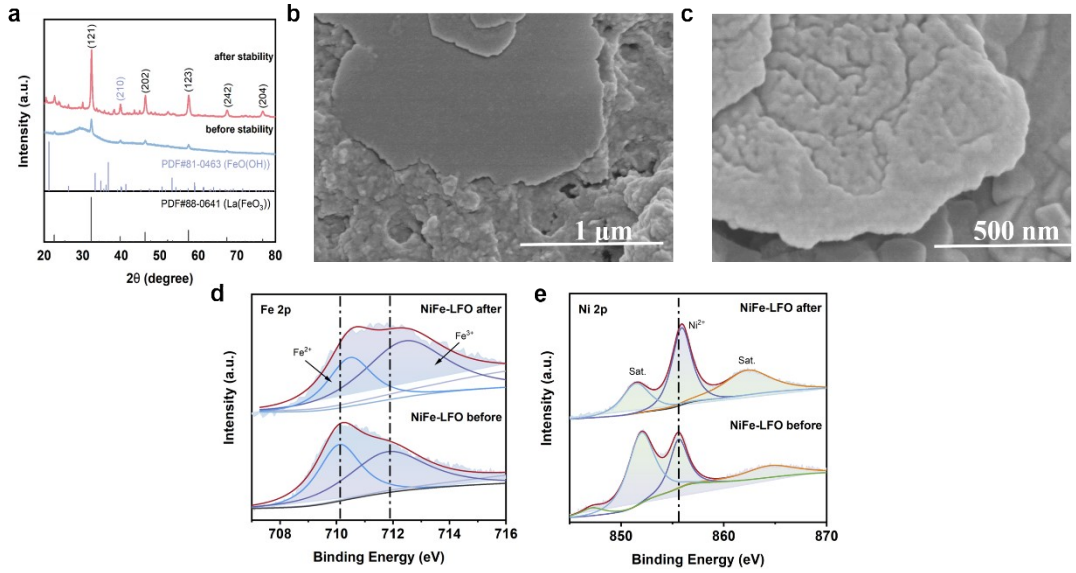

Figure S10. (a) The XRD patterns of NiFe-LFO; (b, c) SEM images of NiFe-LFO; (d, e) High-resolution XPS spectra of (d) Fe, (e) Ni in the NiFe-LFO before and after 48 h galvanostatic conditioning at an anodic current density of 100 mA cm^{-2} in 1 M KOH for OER.

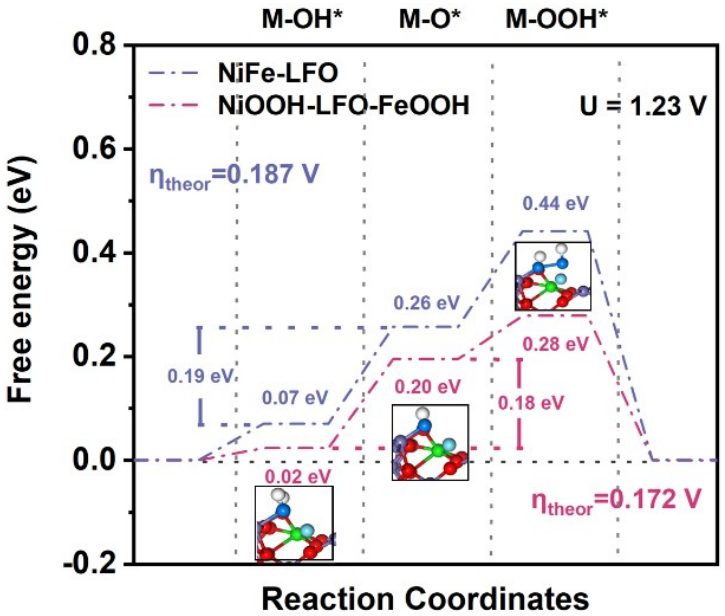

Figure S11. The alkaline OER pathway at U = 1.23 V of NiOOH-LFO-FeOOH and NiFe-LFO

Table S1. Comparison of OER performance of NiFe-LFO with perovskite oxides based OER catalysts

Material	Support	η_{10} (mV)	Taffel Slope (mV dec^{-1})	Reference
NiFe-LFO	NF	186	36.1	**This work**
$LaCoO_3$	NF	342	61	[1]
LCFO	NF	350	59	[2]
BSCF	NF	460	70	[3]
$FeMoO_4$	NF	293	99	[4]
$SmFe_{1-x}Er_xO_3$	NF	184	77	[5]
$CeO_2/LaFeO_3$	RDE	330	67.3	[6]
Si-SCO	RDE	437	66	[7]
SP/DP	GC	268	--	[8]
$LaNiO_3$	GC	~630	84	[9]
LOMO-1	GC	~300	58	[10]
$PrBaCo_2O_{5.75}$	GC	360	70	[11]
SFCMN	Carbon	310	56	[12]
$LaFeO_3$	RDE	510	92	[13]
$SCFW_{0.4}$-BM	RDE	357	58	[14]
F-BSCF	RDE	280	102.7	[15]
V-LCO-II	GC	306	40.0	[16]
BC1.5 MN	RDE	400	70	[17]
CoNi-P	GC	273	45	[18]
$CoFe_2O_4$	GC	341	107	[19]

NF: Ni Foam; RDE: rotating-disk electrode; GC: glassy carbonLCFO: $LaCo_{0.8}Fe_{0.2}O_3$;

BSCF: $Ba_{0.5}Sr_{0.5}Co_{0.8}Fe_{0.2}O_{3-\delta}$; Si-SCO: $SrCo_{1-y}SiyO_{3-\delta}$;

SP/DP: $SrFe_{0.57}Co_{0.27}Mo_{0.16}O_{2.99}/Sr_2Fe_{0.85}Co_{0.17}Mo_{0.56}Ni_{0.42}O_6$

LOMO-1: La_2NiMnO_6 calcined at 700°; SFCMN: 4-$Sr_2Fe_{0.8}Co_{0.2}Mo_{0.65}Ni_{0.35}O_6$;

$SCFW_{0.4}$-BM: $SrCo_{0.4}Fe_{0.2}W_{0.4}O_{3-\delta}$

F-BSCF: F substituted $Ba_{0.5}Sr_{0.5}Co_{0.8}Fe_{0.2}O_{3-\delta}$*;* SNCF-NRs: $SrNb_{0.1}Co_{0.7}Fe_{0.2}O_{3-\delta}$ perovskite nanorods;

V-LCO-II: $LaCo_{0.8}V_{0.2}O_3$

Reference

1. T. Zhao, Y. Wang, X. Chen, Y. Li, Z. Su and C. Zhao, *ACS Sustainable Chemistry & Engineering*, 2020, **8**, 4863-4870.

2. B. Q. Li, C. Tang, H. F. Wang, X. L. Zhu and Q. Zhang, *Science advances*, 2016, **2**, e1600495.

3. G. Chen, W. Zhou, D. Guan, J. Sunarso, Y. Zhu, X. Hu, W. Zhang and Z. Shao, *Science advances*, 2017, **3**, e1603206.

4. Y. Gou, Q. Liu, Z. Liu, A. M. Asiri, X. Sun and J. Hu, *Inorganic Chemistry Frontiers*, 2018, **5**, 665-668.

5. P. Ilanchezhiyan, G. Mohan Kumar, C. Siva, T. W. Kang and D. Y. Kim, *International Journal of Energy Research*, 2020, **45**, 3955-3965.

6. Y. Dai, J. Yu, Z. Zhang, C. Cheng, P. Tan, Z. Shao and M. Ni, *ACS Appl Mater Interfaces*, 2021, **13**, 2799-2806.

7. Y. Pan, X. Xu, Y. Zhong, L. Ge, Y. Chen, J. M. Veder, D. Guan, R. O'Hayre, M. Li, G. Wang, H. Wang, W. Zhou and Z. Shao, *Nat Commun*, 2020, **11**, 2002.

8. H. Sun, B. Hu, D. Guan, Z. Hu, L. Fei, M. Li, V. K. Peterson, H. J. Lin, C. T. Chen, R. Ran, W. Zhou and Z. Shao, *ChemSusChem*, 2020, **13**, 3045-3052.

9. I. Yamada, A. Takamatsu, K. Asai, T. Shirakawa, H. Ohzuku, A. Seno, T. Uchimura, H. Fujii, S. Kawaguchi, K. Wada, H. Ikeno and S. Yagi, *The Journal of*

Physical Chemistry C, 2018, **122**, 27885-27892.

10. Y. Tong, J. Wu, P. Chen, H. Liu, W. Chu, C. Wu and Y. Xie, *J Am Chem Soc*, 2018, **140**, 11165-11169.

11. X. Miao, L. Wu, Y. Lin, X. Yuan, J. Zhao, W. Yan, S. Zhou and L. Shi, *Chem Commun (Camb)*, 2019, **55**, 1442-1445.

12. H. Sun, X. Xu, Z. Hu, L. H. Tjeng, J. Zhao, Q. Zhang, H.-J. Lin, C.-T. Chen, T.-S. Chan, W. Zhou and Z. Shao, *Journal of Materials Chemistry A*, 2019, **7**, 9924-9932.

13. Y. Zhu, W. Zhou, J. Yu, Y. Chen, M. Liu and Z. Shao, *Chemistry of Materials*, 2016, **28**, 1691-1697.

14. G. Chen, Z. Hu, Y. Zhu, Z.-G. Chen, Y. Zhong, H.-J. Lin, C.-T. Chen, L. H. Tjeng, W. Zhou and Z. Shao, *Journal of Materials Chemistry A*, 2018, **6**, 9854-9859.

15. J. Xiong, H. Zhong, J. Li, X. Zhang, J. Shi, W. Cai, K. Qu, C. Zhu, Z. Yang, S. P. Beckman and H. Cheng, *Applied Catalysis B: Environmental*, 2019, **256**.

16. Y. Sun, Z. Zhao, S. Wu, W. Li, B. Wu, G. Liu, G. Chen, B. Xu, B. Kang, Y. Li and C. Li, *ChemSusChem*, 2020, **13**, 2671-2676.

17. H. Sun, J. He, Z. Hu, C.-T. Chen, W. Zhou and Z. Shao, *Electrochimica Acta*, 2019, **299**, 926-932.

18. X. Xiao, C.-T. He, S. Zhao, J. Li, W. Lin, Z. Yuan, Q. Zhang, S. Wang, L. Dai and D. Yu, *Energy & Environmental Science*, 2017, **10**, 893-899.

19. Z. Zhang, J. Zhang, T. Wang, Z. Li, G. Yang, H. Bian, J. Li and D. Gao, *RSC Advances*, 2018, **8**, 5338-5343.